Estimating the Longitudinal Center of Flotation of a Vessel in Waves Using Acceleration Measurements

Nana O. Abankwa, James Bowker, Steven J. Johnston, Mark Scott, and Simon J. Cox

***Abstract*— The location of a vessel's center of flotation during operation at sea plays an important role in the vessel's longitudinal stability. The ability to accurately estimate the location of the center of flotation improves safety monitoring as it indicates how changes in the distribution of weight affect the vessel. In this paper, we propose a novel method for estimating the longitudinal location of a vessel's center of flotation in waves using acceleration readings taken simultaneously at different locations along the length of the vessel. Specifically, we recorded accelerations of an autonomous surface vehicle (ASV) in a towing tank. The ASV was operated in head and following regular waves, which were kept at a constant wave height of 0.12 m while the wave frequency was increased from 0.5 to 0.8 Hz at increments of 0.1 Hz. The results show that multiple acceleration measurements can be used to correctly determine the center of flotation of a vessel in waves. In this experiment, the estimated location of the center of flotation varied as expected based on the longitudinal asymmetry of the ASV and the difference between head and following waves, demonstrating the effectiveness of the proposed method. In addition, the results were validated using the vessel's recorded pitch motion.**

***Index Terms*— Qualisys, accelerometers, center of rotation, center of flotation, vessel safety, vessel stability.**

I. Introduction

DURING operation at sea, knowledge of essential vessel parameters such as the location of the center of flotation, allows operators to objectively make informed decisions regarding vessel stability and safety. Stability is affected by factors including a vessel's weight distribution and the shape of its hull [1]. The continuous redistribution of fuel and water weight during normal operation [2] continuously changes a vessel's trim about its center of flotation [3]. The center of flotation is defined as the center of gravity of a vessel's waterplane area [4].

The interaction of the forces of gravity and buoyancy on a vessel determine its center of rotation. There have been a number of studies investigating the point about which a vessel rotates due to the resultant forces on it during operation [5], [6]. This location is important for many reasons including its effect on a vessel's capsizing probability [7]. Considering the dynamics of rotational motion, a study [8] found the center of rotation when a vessel is pitching or rolling to coincide with the dynamical definition of a vessel's metacenter. The dynamical definition of the metacenter has been shown [6] to coincide with Dupin's [9] and Bougeur's [10], [11] definitions of the metacenter. The use of the metacenter as the center of rotation of a vessel assumes that the center of flotation is fixed [8]. This is not true as the submerged area and the center of this area are constantly changing when a vessel is pitching or rolling. Therefore, in this paper, we will assume the center of oscillatory movement of a vessel pitching or rolling is at the center of flotation [5].

Accelerometers have been applied to a wide range of problems including human activity classification [12], structural vibration monitoring [13] and tilt sensing [14]. A previous study [15] proposed a method for estimating the center of gravity of an aerial vehicle using accelerometers arranged in rings. The chosen approach was validated using a simulation modeling an object subjected to various forces and torques. The proposed method showed the importance of having sufficient angular motion for robust estimation of the location of the center of gravity. This study also demonstrated that more accelerometers improve the estimation. This approach had the disadvantage of requiring knowledge of the aerial vehicle's moment of inertia, mass, and torque. Another study [16] used an approach also involving accelerometers but not arranged in rings to determine the center of gravity of a spacecraft. Both methods mentioned identified the need for the precision of all accelerometers used to be very high, and for there to be sufficient angular motion. They were also both based on the five-term acceleration equation for determining the acceleration of a particle in a rotating reference frame [17]. Even though methods have been developed for determining the center of rotation of spacecrafts and aerial vehicles using accelerometer readings, none have been experimentally applied to a vessel in waves.

Knowledge of significant changes in the center of flotation's location is important because it informs an operator of safety-related issues such as trapped water on deck, which can be dealt with by opening freeing ports. This knowledge can also be used to improve ship handling [18], [19]. The center of flotation is important when loading and unloading a vessel because for a load to have no effect on the vessel's trim, it must be added or removed at the center of flotation [3]. This paper aims to develop a method for applying the five-term acceleration equation to finding the center of flotation of a vessel in waves. The methodology is tested using acceleration readings at multiple points on an autonomous surface vehicle (ASV) in a towing tank. An optical motion capture system is used to

Manuscript received July 6, 2018; revised August 8, 2018; accepted August 10, 2018. Date of publication August 14, 2018; date of current version September 25, 2018. This work was supported by the Engineering and Physical Sciences Research Council under Grant 1368760. The associate editor coordinating the review of this paper and approving it for publication was Prof. Danilo Demarchi. *(Corresponding author: Nana O. Abankwa.)*

The authors are with the Faculty of Engineering and the Environment, Bolderwood Innovation Campus, University of Southampton, Southampton SO16 7QF, U.K. (e-mail: n.abankwa@soton.ac.uk; jab1e08@soton.ac.uk; sjj698@zepler.org; mark.scott@soton.ac.uk; s.j.cox@soton.ac.uk).

Digital Object Identifier 10.1109/JSEN.2018.2865463

Fig. 1. University of Southampton Bolderwood campus towing tank [27].

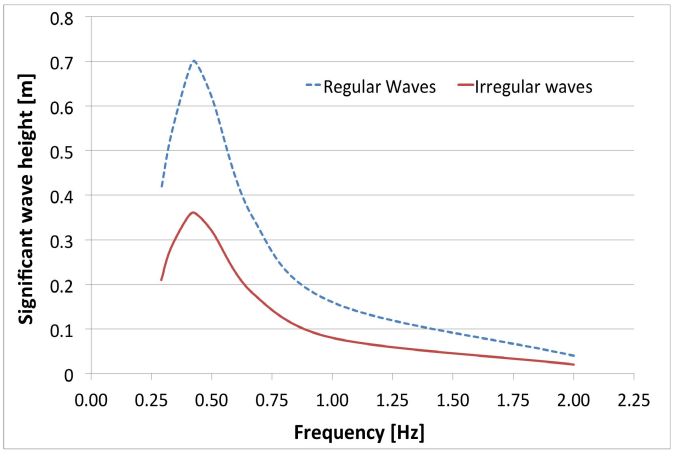

Fig. 2. Wavemaker capability of towing tank [27].

measure the accelerations, and the estimated center of flotation is validated by comparing the maximum and minimum pitch motions computed using the estimated location of the center of flotation with maximum and minimum pitch motions recorded by the optical motion capture system.

The focus of this paper is on the demonstration of a novel data implementation technique for determining the center of flotation of a vessel in waves, which is independent of the data's acquisition method. The proposed method is applicable to acceleration measurements whether they are recorded by optical motion capture systems [20], [21], traditional accelerometers [22]–[24] or a global positioning system [25], [26].

II. Experimental Setup

The data collection process was conducted in the University of Southampton Bolderwood Campus towing tank (Figure 1). The tank is 138 m long, 6 m wide and 3.5 m deep, and has a wavemaker that can model sea states up to 0.7 m significant wave height (Figure 2).

The particulars of the free-running vehicle used are given in Table I. The autonomous surface vehicle, which had two submerged foils for propulsion along the towing tank [28], was tested in head and following regular waves, which were kept at a constant wave height of 0.12 m. The wave frequency was increased from 0.5 Hz to 0.8 Hz at increments of 0.1 Hz as summarized in Table II.

TABLE I
Particulars of the Autonomous Surface Vehicle

Parameter	Value	Units
Length, L	2.27	m
Beam, B	0.30	m
Draft, T	0.10	m
Displacement, Δ	52.00	kg
Chord, c	0.23	m
Span, s	1.00	m
Foil type	NACA0012	-
Foil arm, a	0.40	m

TABLE II
Summary of Details of Runs

Run number	Vessel direction with respect to wavemaker	Wave Amplitude (m)	Wave Frequency (Hz)
1	Towards	0.06	0.50
2	Away	0.06	0.50
3	Towards	0.06	0.60
4	Away	0.06	0.60
5	Towards	0.06	0.70
6	Away	0.06	0.70
7	Towards	0.06	0.80
8	Away	0.06	0.80

The ASV was stationed at the carriage 30 m from the wavemaker and progressed towards the wavemaker in head waves before being turned around and tested in following waves. The period for each run varied from 60 to 180 seconds depending on the forward speed of the ASV and the wave reflection from the opposite end of the tank. During each run, the optical motion capture system (Qualisys) recorded the vessel's pitch and heave displacements and accelerations. The optical motion capture system consisted of eight Oqus 500+ cameras and captured the ASV's motions in six degrees of freedom (DOF) at a rate of 60 Hz. Each camera had a maximum capture distance of 25 m and a 49° horizontal field of vision [29].

As shown in Figure 4, all eight cameras were placed in a row along one side of the towing tank due to practical mounting restrictions. Eight cameras were used to ensure a long coverage volume. This enabled the ASV to remain within the view of the cameras for a sufficient amount of time while it traveled along the length of the towing tank. With the trajectory of the ASV 3.5 m from the cameras, each camera with a horizontal view of 49° covered a length of 3.2 m. Since each unit length was viewed by at least two cameras, the system covered a total length of 12.8 m.

The cameras were daisy-chained and connected to a laptop running the Qualisys Track Manager software (v2.12). This software's graphical user interface (GUI) enables the user to control the cameras' settings, start and stop recording, calibrate the system, and playback recorded runs. A summary of the camera marker settings and video settings used in this setup are presented in Table III.

The Qualisys software computed 3-dimensional (3D) and 6 DOF data from 2-dimensional (2D) marker data. With a

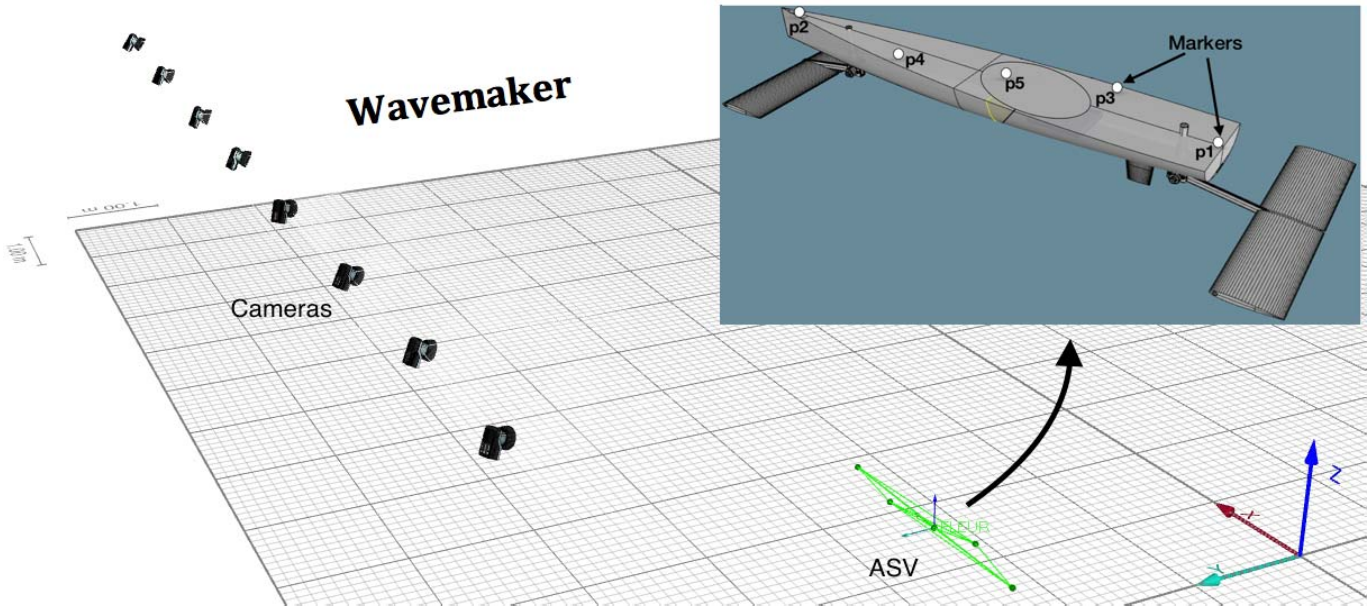

Fig. 3. Experimental setup showing the 8 mounted cameras, the location of the wavemaker, and the position of the markers on the ASV.

TABLE III
QUALISYS CAMERA SETTINGS. (a) MARKER SETTINGS. (b) VIDEO SETTINGS

(a)

Property	Value
Capture rate	60 Hz
Exposure time	0.0005 s
Marker threshold	15 %
Marker type	Passive
Sensor mode	4 MP at 179 Hz

(b)

Property	Value
Capture rate	13 Hz
Exposure time	0.076903 s
Flash time	0.002 s
Gain	4
Sensor mode	4 MP at 179 Hz

measuring volume of 1 × 5 × 10 m, the system provides angular accuracy of 0.05 degrees and spatial accuracy of 0.25 mm [30]. In order for the software to properly compute 3D data from 2D camera images, a wand calibration technique was used to determine the orientations of the cameras. This method used 2 objects to calibrate the optical motion capture system. These objects were an L-shaped structure with 4 markers and a wand with 2 markers. The wand was moved through as many different positions and orientations as possible through the volume the ASV was expected to operate in, with the cameras recording at 100 Hz. The L-frame was fixed throughout the experiment to determine the reference frame. Once the calibration was completed, when tracking markers, the system determined the 3D location of a marker $\begin{bmatrix} X_{\text{world}} & Y_{\text{world}} & Z_{\text{world}} & 1 \end{bmatrix}^T$ from the 2D camera image $\begin{bmatrix} x_{\text{camera}} & y_{\text{camera}} & 1 \end{bmatrix}^T$ using the pin-hole camera model

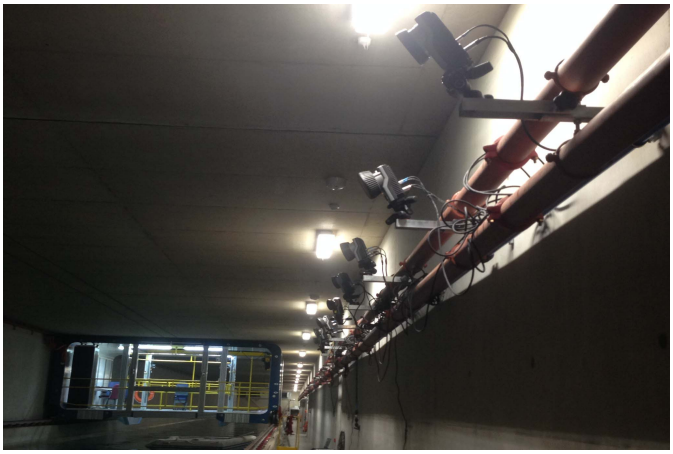

Fig. 4. Arrangement of cameras in towing tank.

[31]–[33] represented in Equation 1.

$$\begin{bmatrix} x_{\text{camera}} \\ y_{\text{camera}} \\ 1 \end{bmatrix} = K \times [R \mid t] \times \begin{bmatrix} X_{\text{world}} \\ Y_{\text{world}} \\ Z_{\text{world}} \\ 1 \end{bmatrix} \tag{1}$$

where

K, is a 3 × 3 intrinsic camera property matrix,
R, is a 3 × 3 extrinsic rotation matrix,
t, is a 3 × 1 extrinsic translation matrix, and
×, indicates the cross product of 2 matrices.

The optical motion capture system's reference frame is shown in Figure 3 with the positive x-direction being towards the wavemaker, the positive y-direction being towards the mounted cameras, and the positive z-direction being upwards. Figure 3 also shows the location of the five markers which indicate the locations of the acceleration readings. The markers were placed asymmetrically to enable the optical motion capture system to better distinguish between them,

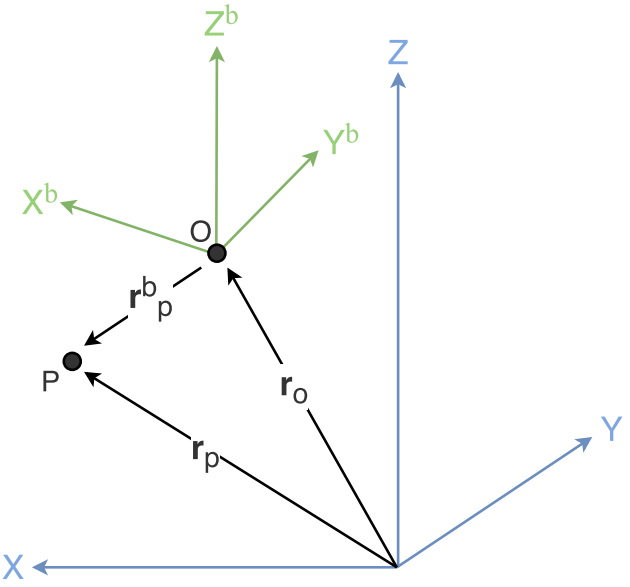

Fig. 5. A translating, rotating reference frame (a vessel, $X^bY^bZ^b$) in a fixed reference frame (flat non-rotating Earth, XYZ)

and for unique definition of the ASV's orientation. Two of the markers were placed at each end of the ASV (the longitudinal limits of the location of the center of rotation). This ensured that there was at least one marker on either side of the center of flotation. Five markers were used in total as four markers are recommended for redundancy, with at least three required to define the ASV as a rigid body [34].

III. Underlying Theory

The method for estimating the center of rotation of a vessel in waves using accelerometers is based on the concept of the acceleration of a point in a rotating coordinate system [35], [36]. Figure 5 shows the general case of a rotating coordinate system centered at point O (a vessel, $X^bY^bZ^b$) and a fixed coordinate system (flat non-rotating Earth, XYZ) being related by translation and rotation.

The measurements of an accelerometer at point P can be calculated as:

$$\mathbf{a}_P = \mathbf{a}_O + (\dot{\boldsymbol{\omega}} \times \mathbf{r}_P^b) + \boldsymbol{\omega} \times \left(\boldsymbol{\omega} \times \mathbf{r}_P^b\right) + (2\boldsymbol{\omega} \times \mathbf{v}_P^b) + \mathbf{a}_P^b - \mathbf{F}_{ext} \tag{2}$$

where

$\mathbf{a}_P$, is the inertial acceleration of point P,
$\mathbf{a}_O$, is the inertial acceleration of point O,
$\boldsymbol{\omega}$, is the angular velocity of the body,
$\dot{\boldsymbol{\omega}}$, is the angular acceleration of the body,
$\mathbf{r}_P^b$, is the displacement from point O to point P,
$\mathbf{a}_P^b$, is the acceleration of point P relative to point O,
$\mathbf{v}_P^b$, is the velocity of point P relative to point O,
$\times$, indicates the cross product of 2 vectors, and
$\mathbf{F}_{ext}$, is any additional acceleration due to external forces such as gravity.

Assuming point O and point P do not move within the body, there is no relative acceleration and no relative velocity between point O and point P in the translating, rotating reference frame ($\mathbf{a}_P^b = 0$ and $\mathbf{v}_P^b = 0$). Equation 2 is reduced to

$$\mathbf{a}_P = \mathbf{a}_O + (\dot{\boldsymbol{\omega}} \times \mathbf{r}_P^b) + \boldsymbol{\omega} \times \left(\boldsymbol{\omega} \times \mathbf{r}_P^b\right) - \mathbf{F}_{ext} \tag{3}$$

Equation 3 is simplified by replacing the cross product operation with the equivalent skew-symmetric matrices [37].

$$\mathbf{a}_P = \mathbf{a}_O + (\mathbf{H}_1 + \mathbf{H}_2)\mathbf{r}_P^b - \mathbf{F}_{ext} \tag{4}$$

where

$$\mathbf{H}_1 = \begin{bmatrix} 0 & -\dot{\omega}_z & \dot{\omega}_y \\ \dot{\omega}_z & 0 & -\dot{\omega}_x \\ -\dot{\omega}_y & \dot{\omega}_x & 0 \end{bmatrix}$$

$$\mathbf{H}_2 = \begin{bmatrix} -(\omega_y^2 + \omega_z^2) & \omega_x\omega_y & \omega_x\omega_z \\ \omega_x\omega_y & -(\omega_x^2 + \omega_z^2) & \omega_y\omega_z \\ \omega_x\omega_z & \omega_y\omega_z & -(\omega_x^2 + \omega_y^2) \end{bmatrix}$$

If all accelerations due to external forces on a rotating, translating body are known, the inertial acceleration at point P on the body can be determined using Equation 4 if the acceleration at point O on the body, the displacement between the two points, the angular acceleration and the angular velocity of the body are known.

In this experimental setup, $\mathbf{H}_1$ and $\mathbf{H}_2$ are common to all of the marker locations since markers 1, 2, 3, 4 and 5 are all on the same body. Using Equation 4 and only accelerometer information from a single marker to estimate the location of the center of rotation is impossible as this requires knowledge of all external forces, the acceleration at the center of rotation, the angular velocity, and the angular acceleration measurements used in calculating $\mathbf{H}_1$ and $\mathbf{H}_2$.

In order to simplify the problem and eliminate the requirement of knowing all the external forces on the ASV, the acceleration measurements at points 2, 3, 4, and 5 are subtracted from the acceleration measurements at point 1 as depicted in Equation 5.

$$\begin{aligned} \mathbf{a}_1 - \mathbf{a}_i &= (\mathbf{H}_1 + \mathbf{H}_2)(\mathbf{r}_1^b - \mathbf{r}_i^b) \\ \mathbf{a}_1 - \mathbf{a}_i &= \mathbf{H}(\mathbf{r}_1^b - \mathbf{r}_i^b) \qquad i = 2, 3, 4, 5 \end{aligned} \tag{5}$$

From Equation 5, $\mathbf{H}$ can be determined since the acceleration measurements and positions of the 5 markers are known. Equation 5 is solved using an ordinary least squares regression [38] without an intercept when rewritten as

$$\begin{aligned} \mathbf{r}_1^b - \mathbf{r}_i^b &= \mathbf{H}^{-1}(\mathbf{a}_1 - \mathbf{a}_i) \\ \begin{bmatrix} x_1^b - x_i^b \\ y_1^b - y_i^b \\ z_1^b - z_i^b \end{bmatrix} &= \begin{bmatrix} h_{11}^{-1} & h_{12}^{-1} & h_{13}^{-1} \\ h_{21}^{-1} & h_{22}^{-1} & h_{23}^{-1} \\ h_{31}^{-1} & h_{32}^{-1} & h_{33}^{-1} \end{bmatrix} \begin{bmatrix} \ddot{x}_1 - \ddot{x}_i \\ \ddot{y}_1 - \ddot{y}_i \\ \ddot{z}_1 - \ddot{z}_i \end{bmatrix} \end{aligned}$$

$$\text{Relative position} = \text{Coefficient} \times \text{Relative acceleration} \tag{6}$$

An alternative approach to solving for the location of the center of flotation using accelerometer readings is to reformulate the regression problem as a linear state-space model, solved using Kalman filters [39], [40].

Equation 6 assumes that the x, y, and z components of the relative acceleration need to interact with each other to produce significant relationships with the x, y, and z components of the relative position. However this is not true because there was

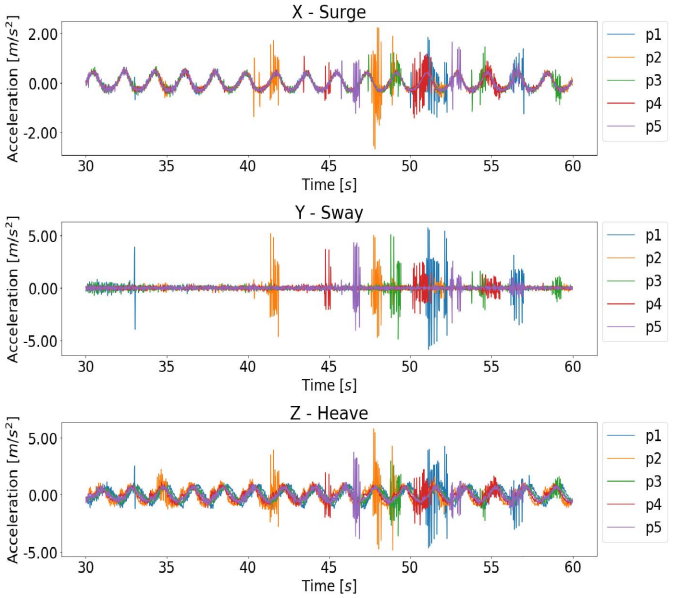

Fig. 6. Raw unfiltered acceleration measurements of markers 1, 2, 3, 4 and 5.

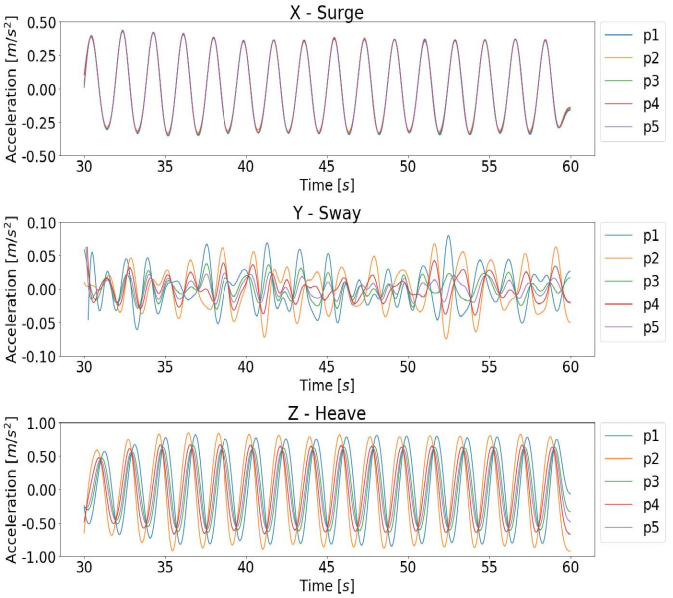

Fig. 7. Acceleration measurement of markers 1, 2, 3, 4 and 5 after filtering.

minimal roll motion so the problem will be considered as a set of simple regression equations.

$$
\begin{aligned}
x_1^{\mathrm{b}} - x_{\mathrm{i}}^{\mathrm{b}} &= h_{11}^{-1} \cdot (\ddot{x}_1 - \ddot{x}_{\mathrm{i}}) \\
x_1^{\mathrm{b}} - x_{\mathrm{i}}^{\mathrm{b}} &= h_{12}^{-1} \cdot (\ddot{y}_1 - \ddot{y}_{\mathrm{i}}) \\
x_1^{\mathrm{b}} - x_{\mathrm{i}}^{\mathrm{b}} &= h_{13}^{-1} \cdot (\ddot{z}_1 - \ddot{z}_{\mathrm{i}}) \\
y_1^{\mathrm{b}} - y_{\mathrm{i}}^{\mathrm{b}} &= h_{21}^{-1} \cdot (\ddot{x}_1 - \ddot{x}_{\mathrm{i}}) \\
y_1^{\mathrm{b}} - y_{\mathrm{i}}^{\mathrm{b}} &= h_{22}^{-1} \cdot (\ddot{y}_1 - \ddot{y}_{\mathrm{i}}) \\
y_1^{\mathrm{b}} - y_{\mathrm{i}}^{\mathrm{b}} &= h_{23}^{-1} \cdot (\ddot{z}_1 - \ddot{z}_{\mathrm{i}}) \\
z_1^{\mathrm{b}} - z_{\mathrm{i}}^{\mathrm{b}} &= h_{31}^{-1} \cdot (\ddot{x}_1 - \ddot{x}_{\mathrm{i}}) \\
z_1^{\mathrm{b}} - z_{\mathrm{i}}^{\mathrm{b}} &= h_{32}^{-1} \cdot (\ddot{y}_1 - \ddot{y}_{\mathrm{i}}) \\
z_1^{\mathrm{b}} - z_{\mathrm{i}}^{\mathrm{b}} &= h_{33}^{-1} \cdot (\ddot{z}_1 - \ddot{z}_{\mathrm{i}})
\end{aligned}
\tag{7}
$$

For a given location on the vessel, Equation 7 shows that to estimate the x, y, and z components of a point's position relative to marker 1, a significant relationship is required with only the x, y, or z component of the point's relative acceleration. Once the coefficient $h_{\mathrm{ij}}^{-1}(\mathrm{i} = 1, 2, 3$ and $\mathrm{j} = 1, 2, 3)$ is known, using Equation 7, the difference in acceleration between two points can be used to compute the relative displacement between the two points.

IV. Results and Discussion

The data from Run 1 (head seas, 0.06 m, 0.50 Hz) is used to illustrate how $\mathbf{H}^{-1}$ was found and the center of flotation was computed starting with the raw unfiltered acceleration measurement at points 1, 2, 3, 4 and 5 (Figure 6).

Figure 6 shows that there was high-frequency noise in the acceleration measurements. A high-order low-pass Butterworth filter was used to reduce the noise and remove outliers [41]. After filtering, the noise was reduced as seen in Figure 7. As seen in Equation 5, the method for estimating the center of rotation of the ASV using only accelerometer measurements involves considering the difference between acceleration measurements at different positions on the ASV.

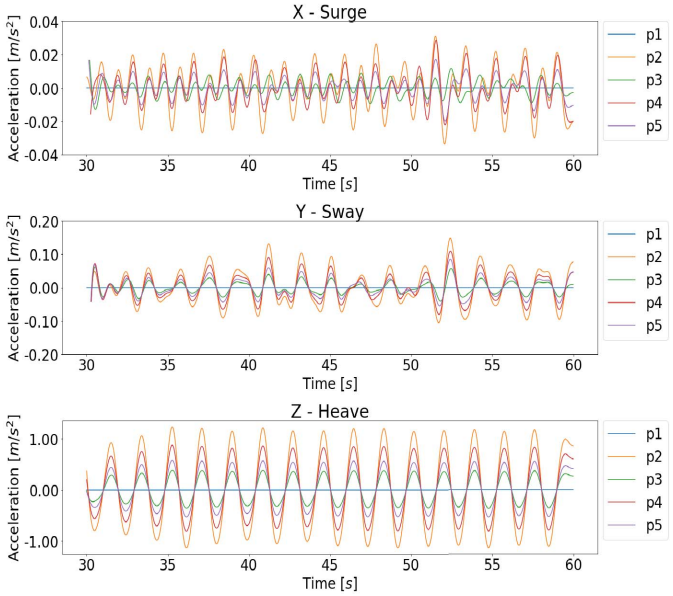

Fig. 8. Acceleration measurements for all markers relative to accelerations at marker 1.

The filtered acceleration measurements for all markers were subtracted from the measurements from marker 1 to obtain data corresponding with Equation 5 (Figure 8).

In Figure 8, as expected the relative accelerations at point 1 were 0. Figure 8 shows that at certain moments in time, all the positions had the same acceleration measurements (relative acceleration = 0). To ensure that the data used in estimating the center of flotation included only times when there was sufficient rotational motion, a peak finding algorithm [42] was used to find peaks in the relative acceleration measurements. Data was selected to include only the times at which the peaks occurred since we only wanted measurements

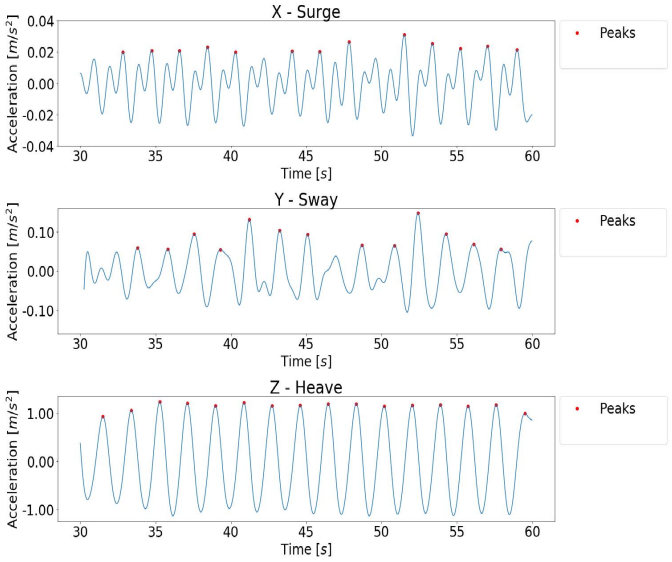

Fig. 9. Peak detection - Marker 2 relative acceleration measurements.

at times when the acceleration measurements were different due to rotational motion. In the z component of the computed relative accelerations, the peaks corresponded to when the ASV was at its maximum pitch angle upwards and the troughs corresponded to the maximum pitch angle downwards.

The peak identification algorithm can be utilized on the data from any of the markers as the peaks occurred at the same time in all the marker positions. Figure 9 shows the peaks identified in the data from marker 2 in Run 1.

Figure 9 shows that the largest values of relative acceleration were in the z-axis. The identified peaks, when the ASV was at its maximum pitch angles, were used to estimate the location of the center of flotation by using the set of simple regression equations shown in Equation 7 to compute the coefficient values in $\mathbf{H}^{-1}$. The coefficient values in $\mathbf{H}^{-1}$ obtained from the regression are presented in Table IV.

In Table IV, the adjusted r-squared column shows how well the regression approximated the real data and was used together with the t-value to select which values in $\mathbf{H}^{-1}$ were used in estimating the center of rotation. These values were also useful for statistically evaluating the solution. The results reflected conclusions in earlier studies showing that when using Equation 3 to estimate the center of flotation, angular motion is required. Since the vessel was in head waves, there was very little roll and yaw angular motion. Pitch motion occurred about the y-axis and was the major source of angular motion, resulting in all h_{ij}^{-1} values found involving the y components of relative position being poor estimates. Since the regression results showed a poor relationship between all relative acceleration values and the y components of relative position for this experimental setup, only the x and z components of the relative position of the center of flotation were estimated using h_{13}^{-1} and h_{33}^{-1} respectively as seen in Equation 8.

$$\begin{aligned} x_1^{\mathrm{b}} - x_{\mathrm{i}}^{\mathrm{b}} &= h_{13}^{-1} \cdot (\ddot{z}_1 - \ddot{z}_{\mathrm{i}}) \\ z_1^{\mathrm{b}} - z_{\mathrm{i}}^{\mathrm{b}} &= h_{33}^{-1} \cdot (\ddot{z}_1 - \ddot{z}_{\mathrm{i}}) \end{aligned} \tag{8}$$

TABLE IV

SUMMARY OF REGRESSION RESULTS. (a) COEFFICIENTS AND STANDARD ERROR VALUES. (b) T AND ADJUSTED r-SQUARED VALUES

(a)

Dependent	H	Independent	Coefficient	Standard Error
$x_1^{\mathrm{b}} - x_{\mathrm{i}}^{\mathrm{b}}$	h_{11}^{-1}	$\ddot{x}_1 - \ddot{x}_{\mathrm{i}}$	-93.7342	3.515
	h_{12}^{-1}	$\ddot{y}_1 - \ddot{y}_{\mathrm{i}}$	-23.3992	1.218
	h_{13}^{-1}	$\ddot{z}_1 - \ddot{z}_{\mathrm{i}}$	-1.9340	0.017
$y_1^{\mathrm{b}} - y_{\mathrm{i}}^{\mathrm{b}}$	h_{21}^{-1}	$\ddot{x}_1 - \ddot{x}_{\mathrm{i}}$	-7.7533	0.604
	h_{22}^{-1}	$\ddot{y}_1 - \ddot{y}_{\mathrm{i}}$	-1.8936	0.211
	h_{23}^{-1}	$\ddot{z}_1 - \ddot{z}_{\mathrm{i}}$	-0.1430	0.014
$z_1^{\mathrm{b}} - z_{\mathrm{i}}^{\mathrm{b}}$	h_{31}^{-1}	$\ddot{x}_1 - \ddot{x}_{\mathrm{i}}$	0.2081	0.090
	h_{32}^{-1}	$\ddot{y}_1 - \ddot{y}_{\mathrm{i}}$	-0.1665	0.053
	h_{33}^{-1}	$\ddot{z}_1 - \ddot{z}_{\mathrm{i}}$	-0.0931	0.001

(b)

Dependent	H	Independent	t	Adjusted R-Squared
$x_1^{\mathrm{b}} - x_{\mathrm{i}}^{\mathrm{b}}$	h_{11}^{-1}	$\ddot{x}_1 - \ddot{x}_{\mathrm{i}}$	-26.670	0.932
	h_{12}^{-1}	$\ddot{y}_1 - \ddot{y}_{\mathrm{i}}$	-19.203	0.876
	h_{13}^{-1}	$\ddot{z}_1 - \ddot{z}_{\mathrm{i}}$	-112.870	0.995
$y_1^{\mathrm{b}} - y_{\mathrm{i}}^{\mathrm{b}}$	h_{21}^{-1}	$\ddot{x}_1 - \ddot{x}_{\mathrm{i}}$	-12.829	0.759
	h_{22}^{-1}	$\ddot{y}_1 - \ddot{y}_{\mathrm{i}}$	-8.969	0.604
	h_{23}^{-1}	$\ddot{z}_1 - \ddot{z}_{\mathrm{i}}$	-10.460	0.629
$z_1^{\mathrm{b}} - z_{\mathrm{i}}^{\mathrm{b}}$	h_{31}^{-1}	$\ddot{x}_1 - \ddot{x}_{\mathrm{i}}$	2.317	0.078
	h_{32}^{-1}	$\ddot{y}_1 - \ddot{y}_{\mathrm{i}}$	-3.116	0.143
	h_{33}^{-1}	$\ddot{z}_1 - \ddot{z}_{\mathrm{i}}$	-90.629	0.992

In order to estimate the location of the center of rotation, the acceleration measurements from marker 2 were used since this marker had the largest acceleration measurements. Assuming the center of flotation was at a point, C, Equation 8 is rewritten as

$$\begin{aligned} x_2^{\mathrm{b}} - x_{\mathrm{C}}^{\mathrm{b}} &= h_{13}^{-1} \cdot (\ddot{z}_2 - \ddot{z}_{\mathrm{C}}) \\ z_2^{\mathrm{b}} - z_{\mathrm{C}}^{\mathrm{b}} &= h_{33}^{-1} \cdot (\ddot{z}_2 - \ddot{z}_{\mathrm{C}}) \end{aligned} \tag{9}$$

To calculate the position of the center of flotation using Equation 9, we needed to know the acceleration at the center of flotation. To achieve this the following points were considered about the vessel:

- The rotational motion at the center of rotation was always zero.
- In the z-axis, the maximum and minimum acceleration readings at the center of rotation occurred when all points on the ASV had the same acceleration.
- In the z-axis, the acceleration of the center of rotation of the ASV was zero when the absolute relative acceleration between two locations on the ASV were at a maximum as shown in Figure 10.

Based on the stated points, we deduced that the times when the acceleration of the center of rotation was temporarily zero coincided with when the peaks in relative acceleration occurred (the difference in acceleration measurements at two ends of the body were at a maximum).

Using the deduced times when the acceleration at the center of flotation was zero and Equation 9, the average location of the center of flotation when the ASV was at its minimum angle was calculated as 103.1 cm $\pm$ 13.9 cm behind marker 2 in the

TABLE V

SUMMARY OF PITCH ANGLES CALCULATED USING DISTANCE OF CENTER OF FLOTATION FROM MARKER 2 ASSUMING UNCORRELATED AND RANDOM ERRORS. (a) HEAD SEAS. (b) FOLLOWING SEAS

(a)

	Minimum pitch angle of ASV[deg]		Maximum pitch angle of ASV[deg]	
Run Number	Computed from relative positions between marker 2 and centre of flotation	Calculated by optical motion capture system	Computed from relative positions between marker 2 and centre of flotation	Calculated by optical motion capture system
1	-2.222 ± 0.008	-2.220 ± 0.050	2.754 ± 0.006	2.734 ± 0.050
3	-2.680 ± 0.005	-2.455 ± 0.050	2.962 ± 0.007	3.226 ± 0.050
5	-2.172 ± 0.005	-1.689 ± 0.050	2.172 ± 0.006	2.658 ± 0.050
7	-1.213 ± 0.005	-0.859 ± 0.050	1.383 ± 0.005	1.670 ± 0.050
Average	-2.064 ± 0.003	-1.806 ± 0.025	2.325 ± 0.003	2.572 ± 0.025

(b)

	Minimum pitch angle of ASV[deg]		Maximum pitch angle of ASV[deg]	
Run Number	Computed from relative positions between marker 2 and centre of flotation	Calculated by optical motion capture system	Computed from relative positions between marker 2 and centre of flotation	Calculated by optical motion capture system
2	-2.406 ± 0.006	-2.970 ± 0.050	3.778 ± 0.008	3.209 ± 0.050
4	-2.795 ± 0.015	-3.465 ± 0.050	3.992 ± 0.009	3.465 ± 0.050
6	-2.270 ± 0.011	-2.914 ± 0.050	2.919 ± 0.013	2.597 ± 0.050
8	-1.243 ± 0.010	-1.825 ± 0.050	2.020 ± 0.011	1.617 ± 0.050
Average	-2.163 ± 0.005	-2.794 ± 0.025	3.194 ± 0.005	2.722 ± 0.025

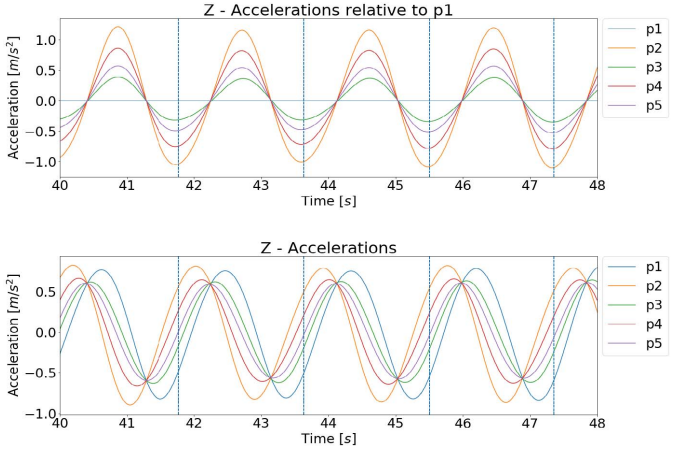

Fig. 10. Acceleration and relative acceleration measurements with times when the acceleration at the center of flotation was zero (vertical dashed line)

x-axis and 4.0 cm ± 0.6 cm below marker 2 in the z-axis. The computed average location of the center of flotation when the ASV was at its maximum angle was 126.8 cm ± 10.7 cm behind marker 2 in the x-axis and 6.1 cm ± 0.6 cm above marker 2 in the z-axis. The uncertainties associated with these values were calculated as the standard errors of prediction of the regression [43] and the uncertainties in the averages are calculated according to error propagation rules [44].

Table VI shows the estimated location of the center of flotation during the eight runs at the maximum and minimum pitch angles. The variations within the uncertainties between

TABLE VI

SUMMARY OF THE CENTER OF FLOTATION'S POSITION RELATIVE TO MARKER 2 FOR EACH RUN. (a) HEAD SEAS. (b) FOLLOWING SEAS

(a)

	At minimum pitch angle		At maximum pitch angle	
Run Number	$x_2^b - x_C^b$ [cm]	$z_2^b - z_C^b$ [cm]	$x_2^b - x_C^b$ [cm]	$z_2^b - z_C^b$ [cm]
1	103.1 ± 13.9	-4.0 ± 0.6	126.8 ± 10.7	6.1 ± 0.6
3	123.9 ± 5.8	-5.8 ± 0.6	123.7 ± 8.3	6.4 ± 0.8
5	129.2 ± 4.8	-4.9 ± 0.6	129.2 ± 8.0	4.9 ± 0.7
7	132.2 ± 7.7	-2.8 ± 0.6	132.5 ± 6.2	3.2 ± 0.7
Average	122.1 ± 4.4	-4.4 ± 0.3	128.1 ± 4.2	5.2 ± 0.4

(b)

	At minimum pitch angle		At maximum pitch angle	
Run Number	$x_2^b - x_C^b$ [cm]	$z_2^b - z_C^b$ [cm]	$x_2^b - x_C^b$ [cm]	$z_2^b - z_C^b$ [cm]
2	116.6 ± 3.7	-4.9 ± 0.7	104.5 ± 6.2	6.9 ± 0.7
4	106.5 ± 15.5	-5.2 ± 1.4	117.5 ± 7.5	8.2 ± 0.9
6	111.0 ± 15.4	-4.4 ± 1.0	111.8 ± 10.7	5.7 ± 1.4
8	110.6 ± 20.0	-2.4 ± 1.0	110.6 ± 18.0	3.9 ± 1.1
Average	111.2 ± 7.5	-4.2 ± 0.5	111.1 ± 5.8	6.2 ± 0.5

the runs were affected by the goodness of fit of the regression to the data in each run. This varied depending on factors including the number of peaks identified, and the range of relative accelerations and positions.

For this experimental setup, the vertical position of the center of mass was not determined because this does not affect the

vessel's longitudinal stability aspect of trim. Considering the center of mass was 129 cm behind marker 2, the results in Table VI show that on average the center of flotation was further behind marker 2 and closer to the center of mass of the ASV in head seas compared to following seas. In Run 7 and Run 8 the z component of the relative position was comparatively low due to the ASV's wave encounter frequency. This reduction in distance was due to a relatively smaller pitch angle as the encounter frequency increased with the wave amplitude remaining constant.

The results were given with respect to a marker rather than the center of mass because during a vessel's operation at sea, the center of mass changes as weights change on board. On the contrary, the locations of acceleration measurements on a vessel remain fixed and serve as an appropriate reference point. These results were validated by using the computed displacement between the center of flotation and marker 2 to calculate the ASV pitch angle using Equation 10.

$$\theta = \tan^{-1}\left(\frac{z_2^{\mathrm{b}} - z_{\mathrm{C}}^{\mathrm{b}}}{x_2^{\mathrm{b}} - x_{\mathrm{C}}^{\mathrm{b}}}\right) \tag{10}$$

The errors associated with the distances, $z_2^{\mathrm{b}} - z_{\mathrm{C}}^{\mathrm{b}}$ and $x_2^{\mathrm{b}} - x_{\mathrm{C}}^{\mathrm{b}}$, were assumed to be uncorrelated and random [44]. These values were compared with the angles measured by the optical motion capture system as shown in Table V. In head seas, the minimum pitch angles from the optical motion capture system were lower than the computed angles and the maximum pitch angles from the optical motion capture system were higher than computed. The opposite was observed in following seas. Upon examination of the experimental setup this was found to be due to a systematic error from the L-frame, which determined the optical motion capture system's reference frame. The L-frame was not absolutely parallel to the still water surface. With the L-frame angled slightly upwards (less than 1 degree) towards the wavemaker, Qualisys overestimated the upwards pitch when the ASV was heading towards the wavemaker and underestimated the downwards pitch. This was opposite when the ASV was heading away from the wavemaker; the upwards pitch was underestimated and the downwards pitch was overestimated.

The results are comparable and show that the absolute value of the maximum pitch was usually greater than the absolute value of the minimum pitch. This is expected due to the longitudinal asymmetry of the hull causing a difference in the submerged volume when the vessel pitches positively and negatively [45].

V. Conclusion and Future Work

This paper presented a novel technique for estimating the longitudinal center of flotation of a vessel in waves. The proposed method was based on acceleration measurements along the length of the vessel. Table IV showed the importance of sufficient angular motion to robust estimation of the location of the center of rotation. Additional markers can be used to improve the precision of the proposed method for computing the location of the center of flotation.

The proposed solution presented has many potential applications since knowledge of the position of the center of flotation is essential for ensuring proper distribution of weights on a vessel and stability. Compared to approaches for vessels not in waves which assume the center of flotation is fixed, the proposed method does not require knowledge of positions and quantities of weights on board a vessel. This solution can also be developed to assess a vessel's static stability by estimating its metacentric height, similar to previous work applying smartphones to ship stability experiments [46].

A similar experimental setup with roll motion rather that pitch motion can be used to estimate the transverse location of the center of flotation. The acceleration measurements recorded using the optical motion capture system can also be compared with measurements from low-cost off-the-shelf accelerometers. This will enable the presented method to be used at sea with a network of accelerometers without requiring a shore-based setup.

Acknowledgment

The authors would like to thank Bertrand Malas, the towing tank manager, for all his guidance during the data collection process. The dataset used in this paper is available at https://doi.org/10.5258/SOTON/D0534.

References

[1] R. Poku, T. W. Oyinki, C. A. N. Johnson, and E. A. Ogbonnaya, "The effects of weight changes on ship's stability," *Brit. J. Appl. Sci. Technol.*, vol. 16, no. 1, pp. 1–9, 2016.

[2] P. Krata, "The impact of sloshing liquids on ship stability for various dimensions of partly filled tanks," *Int. J. Mar. Navigat. Saf. Sea Transp.*, vol. 7, no. 4, pp. 481–489, 2013.

[3] K. J. Rawson and E. C. Tupper, *Basic Ship Theory*, 5th ed. London, U.K.: Butterworth, 2001.

[4] H.-J. Pursey, *Merchant Ship Stability*, 6th ed. Glasgow, U.K.: Brown, Son & Ferguson, 1996.

[5] J. Kliava and J. Mégel, "Non-uniqueness of the point of application of the buoyancy force," *Eur. J. Phys.*, vol. 31, no. 4, p. 741, 2010.

[6] J. Mégel and J. Kliava, "Metacenter and ship stability," *Amer. J. Phys.*, vol. 78, no. 7, p. 738, 2010.

[7] D. Paroka and N. Umeda, "Effect of freeboard and metacentric height on capsizing probability of purse seiners in irregular beam seas," *J. Mar. Sci. Technol.*, vol. 12, no. 3, pp. 150–159, 2017.

[8] J. L. Herder and A. L. Schwab, "On dynamically equivalent force systems and their application to the balancing of a broom or the stability of a shoe box," in *Proc. ASME Design Eng. Tech. Conf. Comput. Inf. Eng. Conf.*, New York, NY, USA, 2004, pp. 1–11.

[9] C. Dupin, *Application de géométrie et de mécanique à la marine, aux ponts et chaussées, etc, pour faire suite aux développements de géométrie*. Paris, France: Bachelier, 1822.

[10] P. Bouguer, *Traité du Navire, de sa construction, et de ses mouvemens*. Paris, France: Jombert, 1746.

[11] H. Nowacki and L. D. Ferreiro, *Historical Roots of the Theory of Hydrostatic Stability of Ships*. Dordrecht, The Netherlands: Springer, 2011, pp. 141–180.

[12] A. Jain and V. Kanhangad, "Human activity classification in smartphones using accelerometer and gyroscope sensors," *IEEE Sensors J.*, vol. 18, no. 3, pp. 1169–1177, Feb. 2018.

[13] A. Sabato, C. Niezrecki, and G. Fortino, "Wireless MEMS-based accelerometer sensor boards for structural vibration monitoring: A review," *IEEE Sensors J.*, vol. 17, no. 2, pp. 226–235, Jan. 2017.

[14] M. Ghanbari and M. J. Yazdanpanah, "Delay compensation of tilt sensors based on MEMS accelerometer using data fusion technique," *IEEE Sensors J.*, vol. 15, no. 3, pp. 1959–1966, Mar. 2015.

[15] Y. M. Al-Rawashdeh, M. Elshafei, and M. F. Al-Malki, "In-flight estimation of center of gravity position using all-accelerometers," *Sensors*, vol. 14, no. 9, pp. 17567–17585, 2014.
[16] Z. Jun, H. He, and L. Yingying, "Spacecraft center of mass online estimation based on multi-accelerometers," in *Proc. 2nd IEEE Int. Conf. Inf. Manage. Eng.*, Chengdu, China, Apr. 2010, pp. 295–298.
[17] J. E. Marsden and T. Ratiu, *Introduction to Mechanics and Symmetry: A Basic Exposition of Classical Mechanical Systems*, 2nd ed. New York, NY, USA: Springer, 1999.
[18] Hapag-Lloyd. (2018). *How Vessel Trim Optimisation Creates Efficiencies*. Accessed: Jun. 27, 2018. [Online]. Available: https://www.hapag-lloyd.com/en/news-insights/insights/2017/03/how-vessel-trim-optimisation-creates-efficiencies.html
[19] K.-H. Su, "Anti-rolling fin control for ship stabilization," in *Proc. Int. Autom. Control Conf. (CACS)*, Dec. 2013, pp. 389–394.
[20] A. Benetazzo, "Accurate measurement of six degree of freedom small-scale ship motion through analysis of one camera images," *Ocean Eng.*, vol. 38, no. 16, pp. 1755–1762, 2011.
[21] E. Nocerino, F. Menna, and F. Remondino, "Comparison between single and multi-camera view videogrammetry for estimating 6dof of a rigid body," *Proc. SPIE*, vol. 9528, p. 95280K, Jun. 2015.
[22] S. Bennett *et al.*, "Measurement of ship hydroelastic response using multiple wireless sensor nodes," *Ocean Eng.*, vol. 79, pp. 67–80, Mar. 2014.
[23] N. O. Abankwa, S. J. Johnston, M. Scott, and S. J. Cox, "Ship motion measurement using an inertial measurement unit," in *Proc. IEEE 2nd World Forum Internet Things (WF-IoT)*, Milan, Italy, Dec. 2015, pp. 375–380.
[24] N. O. Abankwa, G. Squicciarini, S. J. Johnston, M. Scott, and S. J. Cox, "An evaluation of the use of low-cost accelerometers in assessing fishing vessel stability through period of heave motion," in *Proc. Int. Conf. Students Appl. Eng. (ICSAE)*, Newcastle upon Tyne, U.K., Oct. 2016, pp. 59–63.
[25] M. Wolf, G. Liebsch, A. Richter, and R. Dietrich, "Marine motion measurements using GPS," *Int. Hydrographic Rev.*, vol. 4, no. 3, pp. 6–21, 2003.
[26] J. M. Núñez, M. G. Araújo, and I. Garcia-Tuñón, "Real-time telemetry system for monitoring motion of ships based on inertial sensors," *Sensors*, vol. 17, no. 5, p. 948, 2017.
[27] Wolfson Unit. (2016). *Model Basins*. Accessed: Apr. 9, 2018. [Online]. Available: http://www.wumtia.soton.ac.uk/facilities/model-basins
[28] J. Bowker, N. Townsend, M.-Y. Tan, and A. Shenoi, "Experimental analysis of submerged flapping foils; implications for autonomous surface vehicles (ASVs)," in *Proc. MTS/IEEE OCEANS,* Monterey, CA, USA, Sep. 2016, pp. 1–10.
[29] Qualisys Motion Capture Systems. (2018). *Oqus Cameras*. Accessed: Jun. 27, 2018. [Online]. Available: https://www.qualisys.com/cameras/oqus/#tech-specs
[30] Qualisys Motion Capture Systems. (2016). *Qualisys Mocap System Summary and Purchasing Information*. Accessed: Apr. 9, 2018. [Online]. Available: http://teachers.d11.org/teachers/wybrasr/Shared%20Documents/FlightGrantQuotes/QualisysInfo.pdf
[31] O. Faugeras, *Three-Dimensional Computer Vision: A Geometric Viewpoint*. Cambridge, MA, USA: MIT Press, 1994.
[32] K.-Y. Shin and J. H. Mun, "A multi-camera calibration method using a 3-axis frame and wand," *Int. J. Precis. Eng. Manuf.*, vol. 13, no. 2, pp. 283–289, Feb. 2012.
[33] N. A. Borghese and P. Cerveri, "Calibrating a video camera pair with a rigid bar," *Pattern Recognit.*, vol. 33, no. 1, pp. 81–95, 2000.
[34] E. Schoonderwaldt and D. Thompson. (2016). *Learn About 6DOF*. Accessed: Jun. 27, 2018. [Online]. Available: https://www.qualisys.com/webinars/learn-about-6dof/
[35] J. R. Taylor, *Classical Mechanics*. Sausalito, CA, USA: Univ. Science Books, 1997.
[36] S. T. Thornton and J. B. Marion, *Classical Dynamics of Particles and Systems*, 5th ed. Pacific Grove, CA, USA: Brooks/Cole, 2004.
[37] S. Liu and G. Trenkler, "Hadamard, Khatri-Rao, Kronecker and other matrix products," *Int. J. Inf. Syst. Sci.*, vol. 4, no. 1, pp. 160–177, 2008.
[38] J. D. Hamilton, *Time Series Analysis*. Princeton, NJ, USA: Princeton Univ. Press, 1994.
[39] J. Hartikainen and S. Särkkä, "Kalman filtering and smoothing solutions to temporal Gaussian process regression models," in *Proc. IEEE Int. Workshop Mach. Learn. Signal Process.*, Aug./Sep. 2010, pp. 379–384.
[40] S. J. Koopman, "Exact initial Kalman filtering and smoothing for nonstationary time series models," *J. Amer. Stat. Assoc.*, vol. 92, no. 440, pp. 1630–1638, 1997.
[41] S. Butterworth, "On the theory of filter amplifiers," *Exp. Wireless Wireless Engineer*, vol. 7, pp. 536–541, Oct. 1930.
[42] L. H. Negri. (2016). *PeakUtils*. Accessed: Apr. 11, 2018. [Online]. Available: https://pypi.python.org/pypi/PeakUtils
[43] B. Larget. (2007). *Estimation Prediction*. Accessed: May 20, 2018. [Online]. Available: http://www.stat.wisc.edu/courses/st572-larget/Spring2007/handouts03-1.pdf
[44] J. R. Taylor, *An Introduction to Error Analysis*. Sausalito, CA, USA: Univ. Science Books, 2005.
[45] P. Ghadimi, A. Dashtimanesh, S. R. Djeddi, and Y. F. Maghrebi, "Development of a mathematical model for simultaneous heave, pitch and roll motions of planing vessel in regular waves," *Int. J. Sci. World*, vol. 1, no. 2, pp. 44–56, 2013.
[46] M. A. Djebli, B. Hamoudi, O. Imine, and L. Adjlout, "The application of a smartphone in ship stability experiment," *J. Mar. Sci. Appl.*, vol. 14, no. 4, pp. 406–412, 2015.

Nana O. Abankwa received a first-class B.Eng. degree in mechanical engineering from the University of Southampton. He is currently a Postgraduate Research Student with the Computational Engineering and Design Research Group, Faculty of Engineering and the Environment, University of Southampton. He has won a number of competitions including being part of the team that came in first place in the micro-sailboat class of the 2016 World Robotic Sailing Championship and winning the 2017–2018 Rolls-Royce Data Storytelling Challenge. His research project focuses on the methods of acquiring data related to vessel safety using Internet of Things devices. His other interests include data visualization and machine learning.

James Bowker received the M.Eng. degree in ship science/naval engineering from the University of Southampton. He is currently a Postgraduate Research Student with the Faculty of Engineering and the Environment, University of Southampton. His research projects are on wave energy scavenging for autonomous marine systems and energy harvesting utilizing the gyroscopic effect. His research interests include marine renewable energy/sustainable energy systems, seakeeping, bioinspiration/biomimicry, and marine robotics.

Steven J. Johnston received a M.Eng. degree in software engineering from the School of Electronics and Computer Science, University of Southampton, and a Ph.D. degree from the Computational Engineering and Design Group, University of Southampton. He has participated in over 40 outreach and public engagement events as an Outreach Program Manager with Microsoft Research. He is a Senior Research Fellow with the Faculty of Engineering and the Environment, University of Southampton, where he is operating the LoRaWAN wireless network. His current research includes the large-scale deployment of environmental sensors. He is a member of IET.

Mark Scott received a Ph.D. degree in the management of materials engineering and medical research data from the University of Southampton. In 2001, he joined the University of Southampton as an IT Systems Architect and Developer. After working for several groups with the School of Engineering Sciences, he moved to the Central IT Department, where he is currently leading one of its innovation teams. He is interested in the use of IoT devices in research laboratories, including the management and curation of the data and metadata produced. Other interests include data visualization, machine learning, and augmented and virtual reality.

Simon J. Cox received a Ph.D. degree in electronics and computer science and a Degree (First Class) in maths and physics from the University of Southampton. He has won over £30M in research and enterprise funding and industrial sponsorship. He has co-founded two spin-out companies and, as Associate Dean for Enterprise, has most recently been responsible for a team of 100 staff with a £11M per year turnover providing industrial engineering consultancy, large-scale experimental facilities and healthcare services. He is currently a Professor of Computational Methods and the Chief Information Officer with The University of Southampton. He has authored over 250 papers.